PCCP

CrossMark
click for updates

Photocarrier recombination dynamics in ternary chalcogenide CuInS$_2$ quantum dots

Jianhui Sun,[abc] Michio Ikezawa,[c] Xiuying Wang,[a] Pengtao Jing,[a] Haibo Li,[d] Jialong Zhao*[ad] and Yasuaki Masumoto*[c]

Photocarrier recombination dynamics in ternary chalcogenide CuInS$_2$ quantum dots (CIS QDs) was studied by means of femtosecond transient-absorption (TA) and nanosecond time-resolved photoluminescence (PL) spectroscopy. Under strong excitation, the TA dynamics in CIS QDs is well described by a simple rate equation including single-carrier trapping, free-to-bound recombination, and trap-assisted Auger recombination. Under weak excitation, on the other hand, the PL decays of the QDs are composed of a short-lived component caused by surface trapping and a long-lived one caused by free-to-bound recombination. It is found that the surface trapping accelerates markedly with decreasing QD size while the free-to-bound radiative recombination hardly depends on the QD size. Besides this, we observed both a decrease in the PL lifetimes and a dynamic spectral redshift, which are attributed to the surface trapping and the coexistent inhomogeneous broadening in CIS QDs. The spectral redshift becomes less pronounced in CIS/ZnS core/shell QDs because of the suppression of the fast nonradiative recombination caused by the passivation of the surface traps. These results give clear evidence that the free-to-bound model is appropriate for interpreting the optical properties of CIS QDs.

1 Introduction

Quantum dots (QDs) exhibit profound size-dependent opto-electronic properties, having raised widespread concerns in both fundamental science and applications. However, most of the chemically-grown QDs covering the visible and infrared spectrum region are cadmium- or lead-containing materials. Considering environmentally-friendly applications, the chalcopyrite-type I–III–VI$_2$ QDs have been proposed as alternatives because of their less-toxic components. Among them, CuInS$_2$ (CIS) QDs are considered to be one of the most important candidates for optoelectronic devices, because bulk CIS has a direct band gap of 1.53 eV.[1–4] The emission band of CIS QDs can be tuned from the visible to the near infrared regions of the optical spectrum, making them promising semiconductor materials for solar cells,[5–7] light emitting diodes[4,8–10] and bio-labelling.[11–14] Recently, the non-injection thermal-decomposition route has been well developed for the synthesis of CIS QDs and CIS/ZnS (CdS) core/shell QDs.[2,15–18] It has been found that the binary Zn or Cd sulfide

layers passivate the dangling bonds at the QD surface, effectively removing the nonradiative surface trap states.[2,6] Besides this, it was observed that the band gap of CIS QDs can be tuned by introducing the elements of Zn or Cd to form an alloy layer.[19–22] The well-developed synthetic chemistry of CIS QDs opens the door for a large variety of theoretical studies which provide further insight into the potential applications of these QDs.

The exploration of CIS QDs in photovoltaic devices has been greatly put into practice, such as in introducing an interfacial buffer layer between the TiO$_2$ film and the QD sensitizer,[5] hybrid-sensitization with CdS[5,23] and alloying with Se,[6,24] *etc.* However, some of the strategies derived from CdSe QD-based photovoltaic devices are not compatible with CIS QDs. Unlike CdSe QDs, the CIS QDs have a broad photoluminescence (PL) spectrum, large Stokes shift and a long PL lifetime. It should be worth noting that these features would be expected to serve as the dominant mechanisms supporting some particular applications. However, the physical model of the luminescence mechanism for CIS QDs has not been well clarified yet. The optimal device structures and the device efficiency strongly depend on the luminescence process in the QDs.

Recently, the photocarrier dynamics in CIS QDs have been well studied by time-resolved PL spectroscopy. It has been demonstrated that the radiative recombination in CIS QDs involved a transition associated with the localized intra-gap state, since the PL showed long emission lifetime as well as the large Stokes shift.[2–4] The long emission lifetime is due to the large

[a] State Key Laboratory of Luminescence and Applications, Changchun Institute of Optics, Fine Mechanics and Physics, Chinese Academy of Sciences, Changchun 130033, China. E-mail: zhaojl@ciomp.ac.cn; Tel: +86-431-86176313
[b] University of Chinese Academy of Sciences, Beijing 100039, China
[c] Institute of Physics, University of Tsukuba, Tsukuba 305-8571, Japan. E-mail: masumoto@physics.px.tsukuba.ac.jp; Tel: +81-298-534248
[d] Key Laboratory of Functional Materials Physics and Chemistry of the Ministry of Education, Jilin Normal University, Siping 136000, China

disparity in localization volumes of the electron and the hole, which reduces the spatial overlap of their wavefunctions. Klimov and his colleagues demonstrated that the PL emission in CIS QDs came from the transitions associated with internal defect states.[2] Zhong and his colleagues attributed the long emission lifetime to the recombination of donor–acceptor pairs (DAPs) in CIS QDs.[3] Besides this, they observed the high PL quantum yields (QY) in Cu-poor CIS QDs,[4] suggesting that the PL emission in CIS QDs was associated with copper vacancies. The copper vacancy, with a binding energy of around 100 meV in bulk CIS, acts as an acceptor for radiative recombination in CIS QDs.[15] However, the explanation still leaves unclear the issues around the donor states in CIS QDs.

It was reported that recombination of the DAPs dominated the optical properties of the ternary AgInS$_2$ QDs and one piece of evidence was the observation of a PL redshift with increasing decay times.[25,26] For DAPs, recombination between near pairs is more probable than recombination between distant pairs, which leads to the recombination luminescence shifting to longer wavelengths with time after pulsed excitation. The red-shift of the PL spectrum has been also observed in CIS QDs,[13,16] and the PL lifetime decreased dramatically with decreasing wavelength. Therefore, the PL emission in CIS QDs was assumed to come from the recombination of DAPs. However, Omata and his colleagues observed that the increase in the PL peak energy was as large as 0.17 eV when the diameter of the CIS QDs decreased from 4.1 nm to 2.9 nm.[27] The energy change was too large to be attributed to recombination of DAPs, because the energy increase caused by the coulomb interaction is considered to be less than several tens of meV when the QD size changed from 4.1 to 2.9 nm. They further observed that the size-dependent shift in the emission energy changed in proportion to that of the optical band gap, indicating that the radiative transitions are related to the quantum confined levels. In our previous work, we found that the electron trapping at surface defects increased with decreasing QD size, which significantly reduced the carrier lifetimes of small CIS QDs.[28] The different relaxation behavior was due to the size inhomogeneity in CIS QDs. The relaxation of the carriers is faster in smaller QDs because of the larger density of states of electrons and holes at the surface. Besides, both irregular surface states and coexistence of differently sized particles in CIS QDs obscure the difference in the luminescence mechanism between recombination of DAPs and free-to-bound recombination. Therefore, careful investigations into the optical spectroscopy of CIS QDs need to be further conducted to clarify the physical model of the luminescence mechanism.

Here, dodecanethiol-capped CIS core and CIS/ZnS core/shell QDs were synthesized. The size-dependent absorption and PL spectra of the CIS QDs were measured and discussed. We investigated the photo-carrier recombination dynamics by femtosecond TA and nanosecond time-resolved PL measurements, in an attempt to clarify the origin of the PL in CIS QDs. The photocarrier dynamics obtained from TA was found to depend on the excitation power density and could be well described by a simple rate equation. Furthermore, time-dependent redshifts in

the PL spectra were observed for CIS QDs and were attributed to the size-dependent surface-trapping processes and the coexistent size inhomogeneity.

2 Experimental

2.1 Synthesis of CIS QDs and CIS/ZnS core/shell QDs

The dodecanethiol-capped CIS QDs and CIS/ZnS core/shell QDs were prepared using a method developed by Klimov *et al.* with slight modifications.[2] Briefly, 1 mmol indium acetate and 1 mmol copper iodide were mixed with 10 mL 1-dodecanethiol solution in a three-necked flask. The mixture was degassed under vacuum for 5 min and purged with argon three times. Then the flask was heated up to 120 °C for 20 min until a clear solution was obtained. The temperature was then raised to 230 °C and maintained for 1, 5, 20 and 45 min to grow differently-sized CIS QDs. At the desired size, the reaction was quenched by immersing the flask into an ice bath. The samples were purified three times and finally dispersed in toluene for further measurement. Furthermore, the CIS QDs were coated with a ZnS shell to form core/shell QDs by successive ionic layer adhesion and reaction (SILAR) methods. The zinc precursor was prepared by mixing 2 mmol zinc stearate with 20 mL 1-dodecanethiol and the mixture was heated up to 100 °C until the solution turned colourless. Then 5 mL crude CIS QDs solution diluted by 5 mL 1-dodecanethiol was loaded into a three-necked flask. The solution was heated up to 240 °C. After that, 5 mL zinc precursor was injected into the reaction solution at 240 °C and the reaction temperature was kept at 240 °C for 30 min to grow the first shells. The subsequent injection of the zinc precursor was conducted up to three times, and every time the temperature was kept at 240 °C for 30 min to change the thickness of the shells. The reaction was terminated by cooling down the reaction mixture. Finally, the samples were purified three times and dispersed in toluene for storage.

2.2 Characterization of CIS QDs and CIS/ZnS core/shell QDs

Steady-state PL spectra were recorded by a JASCO F-8500 spectrophotometer. Steady-state absorption spectra were recorded by means of a UV-vis-NIR scanning spectrophotometer (Hitachi U-3300). The average diameters of CIS QDs were determined to be 2.0, 2.5, 3.3, and 4.0 nm, respectively, by means of transmission electron microscopy (TEM) (JEOL JEM-2010F). The powder X-ray diffraction (XRD) patterns shown in Fig. 2(c) were obtained using a Rigaku-2000 diffractometer.

2.3 Femtosecond TA and time-resolved PL spectroscopy

The white-light femtosecond TA spectrometer used in this study is based on a regeneratively-amplified Ti:sapphire laser system (Spectra-Physics, 800 nm, 130 fs, and 1 kHz repetition rate). The pump pulses at 400 nm were generated by frequency doubling of the 800 nm laser beam in a β-barium borate (BBO) crystal 2 mm thick. The white-light probe was generated by focusing the 800 nm laser beam onto a sapphire plate 2 mm thick. The pump pulses were chopped by a synchronized chopper

operated at 25 Hz. After passing through the sample, the probe beam was focused into a fiber-coupled spectrometer (Ocean Optics USB2000+, 300–1100 nm, and 2048 pixels). The angle between the pump and probe polarizations was set at the magic angle (54.6 degrees) to ensure the dynamics was free from reorientation effects. The group velocity dispersion of the whole experimental system was compensated for by a chirp program. Control of the spectrometer was achieved *via* custom-written LabVIEW programs through serial connection. During the data collection, samples were constantly moved in *X–Y* directions at a speed of 10 cm min^{-1} to avoid the degradation of the samples at the excitation spot.

Time-resolved PL was measured by means of a time-correlated single photon counting (TCSPC) system coupled to a JASCO CT-25 monochromator and a Hamamatsu R928 photomultiplier. The samples were excited at 375 nm by a 70 picosecond pulsed diode laser (Hamamatsu PLP-10). Time resolution of the TCSPC system was about one nanosecond.

3 Results and discussion

3.1 Optical and morphological analysis

As shown in Fig. 1(a), the absorption edge and PL band of CIS QDs gradually shifts toward a longer wavelength with increasing QD size, in agreement with the quantum confinement effect. A broad absorption band for all the CIS QDs was observed together
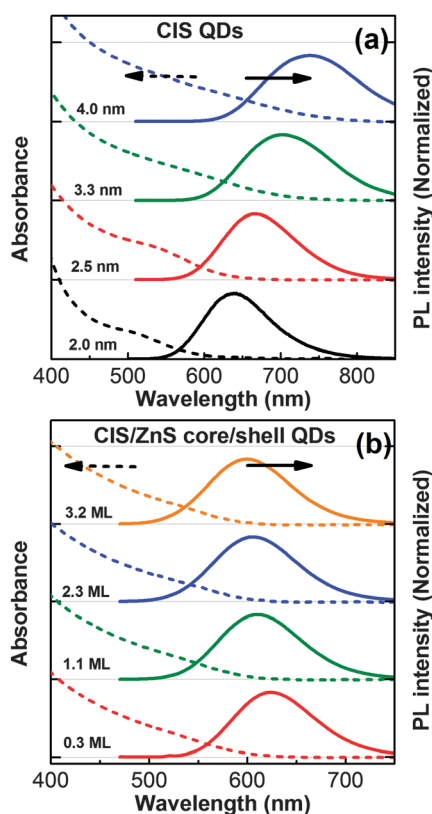

Fig. 1 Steady-state absorption (dashed lines) and PL spectra (solid lines) of (a) CIS QDs of four different sizes and (b) CIS/ZnS core/shell QDs with core diameter of 2.5 nm and ZnS shells of four different thicknesses.

with an absorption tail at the long wavelength side. No sharp absorption peak was observed. It is well known that the presence of discrete electronic states are masked in the linear absorption spectra of the chemically-grown QDs by large inhomogeneous broadening.[3,29] Each QD may vary in size, geometry, and stoichiometry, especially for CIS QDs because of their ternary chemical composition. The ternary CIS QDs may have more complicated lattice imperfections because of the tetragonal lattice distortion and the deviation in stoichiometry. So, the surface states and the intrinsic defects are equally important and can act as potential fluctuations to localize carriers. Like previous reports, the CIS QDs have a very broad PL band with a full width at half maximum (FWHM) of more than 100 nm, which is almost three times that of monodisperse CdSe QDs.[2,3] The broadened PL spectra are due to the distribution of vibrational states and the coexistent size inhomogeneity. The PL band gradually shifts to the longer wavelength, and the low-energy tail of the 4 nm diameter CIS QDs extends below the bulk CIS band-edge. It is indicative of this that the radiative transition does not come from excitonic recombination. This conclusion is further supported by our observation that the emission peaks of the CIS QDs exhibit a long emission lifetime and a large Stokes shift of around 300 meV.

Furthermore, the CIS/ZnS core/shell QDs were synthesized by the SILAR method. The average diameters of the QDs increase after the shell growth as observed from the TEM images in Fig. 2. As shown in Fig. 1(b), both the absorption and PL spectra of the CIS/ZnS core/shell QDs show a blueshift with respect to those of their parent CIS QDs. Li *et al.* attributed the blueshift to the etching of the core materials which increased the degree of spatial confinement.[2] However, Tang *et al.* described the origin of this blueshift as the partial alloying of CIS QDs with ZnS.[20] The explanation for such a blueshift in CIS/ZnS core/shell QDs is still under debate. As shown in Fig. 1(b), the first coating of 1.1 monolayer (ML) ZnS shells on 2.5 nm diameter CIS core QDs resulted in core/shell structures with a significant blueshift in the emission peak from 670 nm to 606 nm. Afterwards, the emission peak of the CIS/ZnS core/shell QDs slowly blue-shifted to 595 nm as the thickness of the ZnS shells increased to 3.2 ML. The large blueshift for the first 1.1 ML shells can be attributed to the partial exchange of Cu^+ and In^{3+} cations with Zn^{2+} cations, because CIS and ZnS have a similar Gibbs formation enthalpy.[19] When a complete ZnS shell was formed, the cation exchange slowed down. The later slow blueshift is due to the diffusion of the Zn into CIS to form an alloy layer. The degree of the alloying slightly increases as time proceeds at high temperature.

As shown in Fig. 2(c), the X-ray diffraction (XRD) patterns of the QDs show that their crystal structure is identical to the tetragonal chalcopyrite structure. The reflection peaks of the CIS QDs positioned at 28.5 degrees, 47.4 degrees, and 55.5 degrees in 2θ can be assigned to the (112), (220)/(204), and (312)/(116) lattice planes, respectively. Since the lattice parameter of chalcopyrite CIS is larger than that of zinc blende ZnS, the reflection peaks of the CIS/ZnS core/shell QDs slightly shifted to a larger 2θ compared to CIS QDs. Besides this, the XRD pattern of the CIS/ZnS core/shell QDs reveals a narrowing of the peaks,

This journal is © the Owner Societies 2015

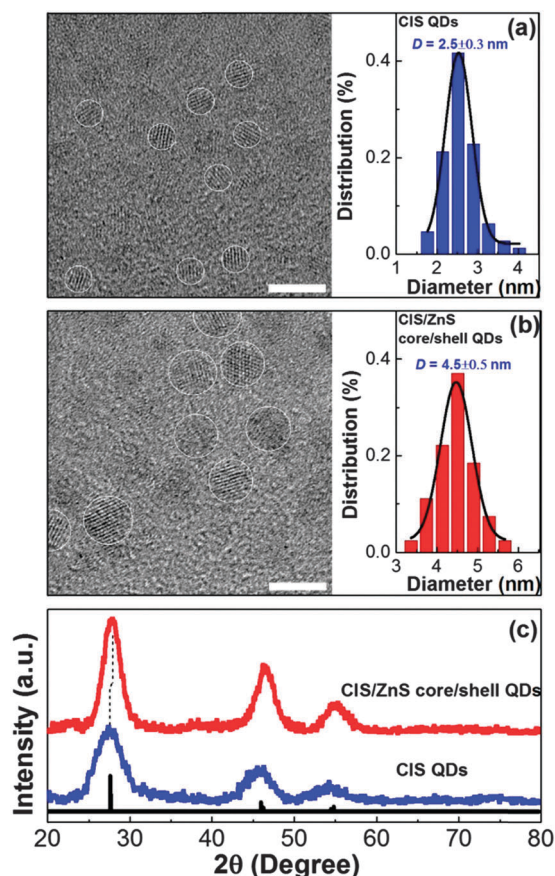*Phys. Chem. Chem. Phys.,* 2015, **17**, 11981–11989 | **11983**

Fig. 2 Transmission electron microscopy images and size distributions of (a) 2.5 nm diameter CIS QDs and (b) CIS/ZnS core/shell QDs with core diameter of 2.5 nm and shell thickness of 3.2 ML. The scale bar is 5 nm. (c) Powder X-ray diffraction patterns of CIS QDs (blue curves) and CIS/ZnS core/shell QDs (red curves). The black solid line is the X-ray diffraction pattern of bulk CIS.

because the size of the CIS/ZnS core/shell QDs increased with respect to their parent CIS QDs.

3.2 Ultrafast TA spectroscopy of CIS QDs

We investigated the laser-intensity dependence of the TA kinetics to understand the dynamics of the photocarriers in CIS QDs. As shown in the inset in Fig. 3(a), a rather symmetrical bleaching band is observed. The bleaching of the absorption is caused by the filling of 1S quantized levels. As seen in Fig. 3(b), the intensity of the bleaching increases with increasing pump fluence and saturates at higher fluence. The saturation indicates that the degeneracy of the 1S transitions is finite in CIS QDs. It has been suggested that the band-edge bleach at room temperature was dominated by the filling of 1S electron states without a discernible contribution from holes in the CIS QDs.[2,27] This is because the degeneracy of the valence band is much larger than that of the conduction band, which is the combined result of a large difference between electron and hole masses ($m_h/m_e = 8$) and the complex multi-subband structure of the valence band in CIS QDs. A similar result has been previously reported for CdSe QDs, where the strong band-edge bleach is dominated by the
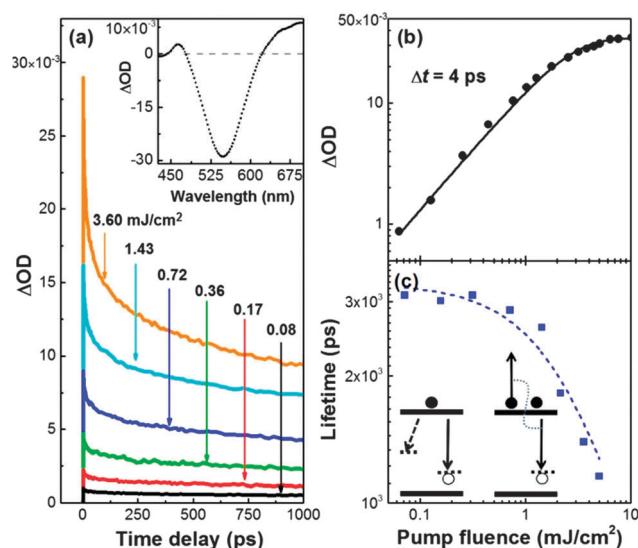

Fig. 3 (a) TA kinetics of 2.5 nm CIS QDs under different excitation densities; the inset shows the TA spectrum under a pump fluency of 3.6 mJ cm^{-2}. Excitation power density dependence of the (b) bleach amplitudes and (c) average life times probed at 1S transitions. The left scheme in figure (c) depicts the surface trapping and free-to-bound recombination under low pump fluency. The right scheme in figure (c) depicts the trap-assisted Auger recombination under high pump fluency. The dashed line in (c) is the fit by eqn (1).

population of the lowest energy 1S electron level.[30] Therefore, it is possible for us to know the dynamics of the 1S electron in CIS QDs by means of TA spectroscopy.

The TA kinetics of 2.5 nm diameter CIS QDs under different excitation densities is shown in Fig. 3(a). Note that we can not accurately characterize TA lifetimes longer than one nanosecond because of the limited length of the delay stage. Below the excitation power density of 1 mJ cm^{-2}, the decay profiles have two decays consisting of a fast decay associated with surface trapping and a slow decay associated with the free-to-bound recombination (left scheme in Fig. 3c). The size-dependent surface-trapping will be discussed later in depth based on the time-resolved PL experiment. Here, we observed another kind of fast decay component that was added to the decay profile when the excitation power density exceeds 1 mJ cm^{-2}. In the case of CdSe QDs, many carriers are present in each QD under high excitation densities and de-excitation occurs through the fast multicarrier Auger process.[30] An example of such an Auger-mediated recombination includes a scenario where one electron–hole (e–h) pair gives its energy to another electron or hole.[31] Recently, this carrier multiplication has also been observed in CuInSe$_2$ QDs.[32] Considering that the PL of CIS QDs is attributed to the recombination of a conduction-band electron and a deeply-trapped hole,[27] the fast-decay component observed here is therefore an indication of the trap-assisted Auger recombination under strong excitation. Trap-assisted Auger recombination has been investigated in bulk silicon.[33] Recently, it was observed and studied in the confined system of ZnO QDs.[31] Trap-assisted Auger recombination in QDs involves the recombination of conduction-band electrons and deeply

trapped holes *via* nonradiative energy transfer to extra conduction-band electrons (right scheme in Fig. 3c).

The average TA-lifetimes as a function of the excitation densities are summarized in Fig. 3(c). The average lifetime decreases in inverse proportion to the excitation power density at excitation power density above 1 mJ cm^{-2}, while it remains almost constant under weak excitation. Such power-dependent dynamics in semiconductors can be well explained by a rate equation that includes single-carrier trapping, free-to-bound recombination, and trap-assisted Auger recombination. When the densities of photoexcited electrons and holes are equal to each other, the rate equation for the photocarriers can be simplified and written as follows: $1/\tau = \alpha + \beta n + \gamma n^2$,[33–35] where n is the photocarrier density and α, β, and γ represent the nonradiative single-carrier-trapping rate, radiative bimolecular recombination coefficient, and nonradiative Auger recombination coefficient, respectively. We assume that the acceptor density (N_h) is much larger than the carrier density; βn and γn^2 can then be written as βN_h and $\gamma N_h n$, respectively, where βN_h and $\gamma n N_h$ represent the decay rate of the free-to-bound radiative recombination and the trap-assisted Auger recombination, respectively.[35–37] Therefore, the TA lifetime under different excitation densities can be approximately written as

$$\tau = 1/(A + Bn), \tag{1}$$

where $A = \alpha + \beta N_h$ and $B = \gamma N_h$. We performed a fitting to the TA lifetime and this expression reproduced well the experimental results as shown in Fig. 3(c). We can not obtain the non-radiative Auger recombination coefficient of γ because of the absence of information about the acceptor density in CIS QDs. From eqn (1), we can show that the lifetime of the CIS QDs will be determined solely by the acceptor density under weak excitation, because the Auger recombination can be neglected. The copper vacancies act as the acceptors in CIS QDs and the qualitative evaluation of the acceptor density on carrier dynamics has been examined by PL spectroscopy.[2,4,28] The density of copper vacancies in CIS QDs is tuned by changing the molar ratio between precursor Cu$^+$ and precursor In^{3+}. Zhong and his colleagues observed that the lifetime of CIS QDs with a [Cu]/[In] molar ratio of 0.4 was shorter than for CIS QDs with a ratio of 0.7,[4] which is consistent with our conclusion from eqn (1). It is because the CIS QDs with a [Cu]/[In] molar ratio of 0.4 have a larger density of copper vacancies than CIS QDs with a ratio of 0.7, and because copper vacancies work as acceptors.

3.3 Time-resolved PL spectroscopy of CIS QDs and CIS/ZnS core/shell QDs

To further understand the photocarrier dynamics in CIS QDs, time-resolved PL spectroscopy was performed. The quantitative study of carrier dynamics provides further understanding of the optical properties of CIS QDs. Fig. 4(a) shows the normalized PL kinetics of four differently-sized CIS QDs. The PL decay profiles have two distinct decay components: the initial fast decay over dozens of nanoseconds followed by a slow decay over hundreds of nanoseconds. It is well known that the CIS QDs have a long emission lifetime of around 300 nanoseconds, which is much
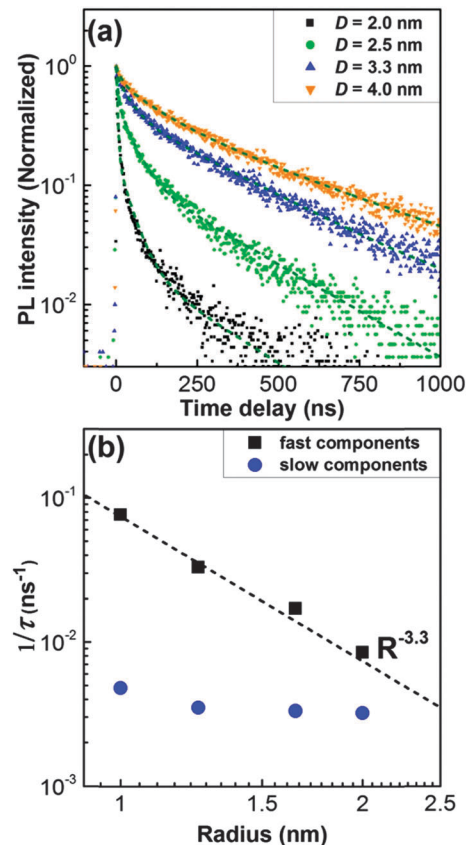

Fig. 4 (a) Normalized PL kinetics of CIS QD samples with four average diameters. The dashed line represents the fit by a three-exponential function. (b) The nonradiative surface trapping rates $1/\tau_{trap}$ and radiative recombination rates $1/\tau_3$ are plotted by the blue circles and the black squares, respectively. The black dashed line represents the fit by a power-law expression.

longer than those of II–VI QDs, such as CdSe QDs, having an exciton lifetime of 10–30 nanoseconds.[3,38] Besides, it is known that the surface defects in QDs, such as the dangling bonds, act as charge acceptors supplying excellent channels for exciton dissociation at the QD surface.[38] The time constants of surface trapping in CIS QDs vary significantly from nanoseconds to sub-100-nanoseconds probably because of the irregular surface states and different sizes. A component of tens of nanoseconds was observed in CIS QDs and was attributed to the nonradiative recombination induced by surface defects.[2] The high probability of carrier trapping at surface defects causes the degradation of QD-based optoelectronic devices. Therefore, surface trapping is an important phenomenon in QDs because it reduces PL quantum efficiencies and obscures the interaction of excitons with their surroundings.

Here, size-dependent surface-trapping over dozens of nanoseconds was observed in CIS QDs. As discussed above, there are two channels for exciton dissociation in CIS QDs. However, the PL kinetics in CIS QDs can not be well fitted by the bi-exponential function, because the time constants for surface trapping have a broad distribution. A quantitative analysis of the PL decay curves was conducted using a three-exponential fit.

As shown in Fig. 4(a), all the decay curves are well fitted by a three-exponential function written as: $A_1 \exp(-t/\tau_1) + A_2 \exp(-t/\tau_2) + A_3 \exp(-t/\tau_3)$. The fit yields time constants τ_1 and τ_2 in dozens of nanoseconds, and the time constant τ_3 in hundreds of nanoseconds. As we discussed above, the initial fast decay over dozens of nanoseconds comes from the surface trapping. Therefore, we calculate the average lifetimes of trapping as: $\tau_{trap} = (A_1 \tau_1^2 + A_2 \tau_2^2)/(A_1 + A_2)$, and the trapping rate is written as $1/\tau_{trap}$. Fig. 4(b) shows a plot of trapping rate $1/\tau_{trap}$ as a function of the average radius (R). The trapping rates increase exponentially as the radius of the CIS QDs decreases. The dashed line in Fig. 4(b) shows the best fit of these data by a power law expression: $1/\tau_{trap} = A \cdot R^n$, where A is the amplitude and n describes the order. The trapping rate follows an $R^{-3.3}$ functional form, as does the fraction of the 1S envelope function at the surface including tunneling.[39] However, the radiative recombination rates $1/\tau_3$ increase slightly with a decrease in QD size. The oscillator strength increases as the size of the CIS QDs becomes smaller than the exciton Bohr radius. In other words, an increase in the oscillator strength should lead to a larger decay rate in the smaller QDs.

As shown in Fig. 5(a), the PL kinetics in CIS QDs are spectrally non-uniform and are significantly faster at the blue side of the emission band than at its red side. This indicates that the short-lived contribution to the PL signal is associated with the higher-energy band, while the longer-lived signal is associated with the lower-energy band. A sum of a three-exponentials function describes all of the PL decay curves very well across the entire emission profile, with variations in amplitude accounting for the spectral dependence of the decay rate. The peak wavelength and width of the time-resolved PL spectra for various delay times are estimated using a Gaussian profile to fit the PL spectrum. As time proceeds, the PL spectrum exhibits both a pronounced redshift and a decrease in the spectral width, as shown in Fig. 5(b). Similar redshift phenomena have been reported for AgInS$_2$ QDs.[25,26] The redshift of the PL band indicates that the different relaxation behavior is associated with the different channels. The spectral redshift in CIS QDs as time proceeds had been previously attributed to the recombination of DAPs.[3,4,15] The recombination between near DAPs is more probable than that between distant DAPs, which leads to the spectral redshift as time proceeds. It was demonstrated that the lifetime of DAPs in quantum confined systems increases with decreasing QD size because of the "exciton dribbling" effect in which the free excitons slowly dissociate into close DAPs.[40] However, our observation that the average lifetime increases with the increase in the QD size contradicts the previous report. As discussed above, the fast surface-trapping in bare CIS QDs increases markedly with a decrease in the size of the QDs. Therefore, the spectral redshift in CIS QDs can be attributed to the size-dependent surface-trapping and the coexistent size inhomogeneity. In smaller CIS QDs, PL emission is observed at the blue side and is mainly associated with short-lived surface traps. The relaxation of the 1S states is faster in smaller QDs with larger densities of carriers at the surface, because the surface trapping rate is proportional to the existing probability of carriers at the QD surface.[28,39] Therefore, surface traps provide local sites for fast relaxation of the photoexcited excitons, mainly resulting in a short PL lifetime for smaller CIS QDs with shorter-wavelength emission.

We investigated the PL kinetics of the CIS QDs before and after shell growth to further understand the luminescence mechanism underlying the extrinsic impurities, as shown in Fig. 6(a). The inset of Fig. 6(a) shows the average lifetimes plotted as a function of ZnS shell thickness. The PL lifetime of CIS/ZnS core/shell QDs exhibits a significant increase with increasing shell thickness. The increase in the PL lifetimes is probably caused by the passivation of surface defects and the spatial separation of electrons and holes. The spatial separation of the electrons and holes is solely caused by the delocalization of the 1S electron into the ZnS shells, because the holes are firmly localized at the internal defects in CIS QDs. In our previous work,[41] the eigenfunction and energy of the electron in CIS/ZnS core/shell QDs were calculated taking into account the radial distribution of the wavefunction for the 1S electron by modelling them as a particle confined in a spherical well of finite depth. We observed that the delocalization of the 1S electron into the ZnS shells is very limited even in case of a thick shell. Therefore, we considered that the significant increase in the PL lifetime of CIS/ZnS core/shell QDs was mainly caused by the passivation of surface defects with the binary ZnS layers. As shown in the inset of Fig. 6(a), the surface passivation suppresses a faster decay and simultaneously improves PL efficiency.
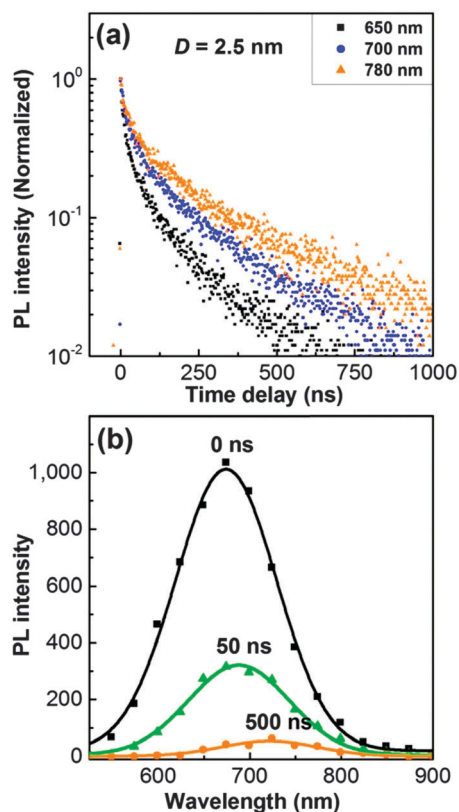

Fig. 5 (a) Normalized PL kinetics of 2.5 nm average diameter CIS QDs at wavelengths of 650, 700 and 780 nm. (b) Time-resolved PL spectra of 2.5 nm CIS QDs at 0, 50 and 500 ns. The solid lines represent the results of the spectral fitting analysis.

11986 | *Phys. Chem. Chem. Phys.,* 2015, **17**, 11981–11989

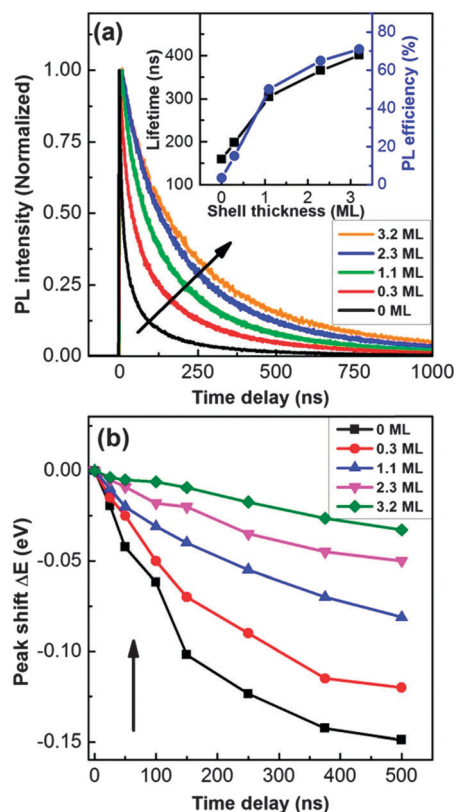This journal is © the Owner Societies 2015

Fig. 6 (a) Normalized PL kinetics of CIS/ZnS core/shell QDs with core diameter of 2.5 nm and various ZnS shell thicknesses. The average lifetimes (black squares) and PL efficiencies (blue circles) are plotted as a function of shell thickness in the inset. (b) Peak energies of the time-resolved PL spectra as a function of the time delay. The PL peak energy at the origin of time is taken to be zero. The black arrows indicate the improving passivation of surface defects by ZnS shells.

This observation confirms that this channel is associated with recombination through a surface trap which primarily serves as a centre for nonradiative decay.

Moreover, we examined the time-resolved PL spectra of CIS/ZnS core/shell QDs. As shown in Fig. 6(b), the temporal peak-shift depends on the ZnS shell thickness. The peak shifts are plotted as a function of the time after excitation by a pulsed-laser. Here, in order to reduce the etching effect that caused the variation in band-gap energy, the peak shifts are evaluated by $\Delta E(t) = E(t) - E_0$, where $E(t)$ and E_0 are the PL peak energy at the time t and at the time of the excitation, respectively. The CIS core QDs show the most dramatic spectral shift, whereas CIS/ZnS core/shell QDs with 3.2 ML shells show little spectral change. The increased shell thickness suppresses surface trap states and the peak shift. The redshifts are less pronounced in CIS/ZnS core/shell QDs because of the suppression of fast surface trapping caused by the passivation of surface defects.

3.4 The analysis of internal defects in CIS QDs

Finally, we discuss the internal defects in CIS QDs. The internal defect states are divided into deep and shallow traps in bulk CIS materials.[42,43] Deep traps are essentially localized at the lattice defects and lie in the middle of the band gap. Shallow traps lie

within a few meV of the corresponding band edge. These defects are suggested to still exist in CIS QDs and to even dominate the luminescence.[15] At deep traps, the carriers are strongly bounded, and the delocalization of the carriers is limited, such as the carriers trapped at the copper vacancies. Copper vacancies had been demonstrated to act as deep acceptors with a large binding energy of more than 100 meV in CIS QDs.[15,28] Besides, it was reported that the size-dependent shift of the emission energy in CIS QDs changed in proportion to that of the optical band gap and the radiative transitions were associated with the quantum confined levels.[27] So, we consider that the quantum confined level contributing to the emission in CIS QDs is conduction-band or shallow trap level. For shallow donors, when the size of the CIS QDs is comparable to or smaller than the donor Bohr radius of 2.8 nm, determined by the effective mass approximation,[44] electrons trapped at the shallow donors are expected to delocalize over the whole QD. The distinction between trapped and free electrons disappears. Similar effects have been demonstrated in CdS QDs.[45,46] Therefore, even if there are shallow donors in CIS QDs, the emission can be attributed to the free-to-bound radiative recombination.

On the basis of the spectroscopic studies described above, a summary of the identified relaxation processes in CIS QDs is illustrated schematically in Fig. 7. As the CIS QD size decreases, shallow acceptor levels shift to higher energy. In CIS QDs smaller than 5.6 nm in diameter, electrons trapped at the shallow donors are expected to delocalize over the whole QD. Therefore, the shallow donor states mix strongly with the conduction band electron states, whereas the deep acceptor states are strongly located at internal defects. The spectral shape of the broad PL is mainly determined by the strong interaction between phonons and holes trapped at the deep acceptors. We consider that the broad PL in the CIS QDs is due to the recombination between
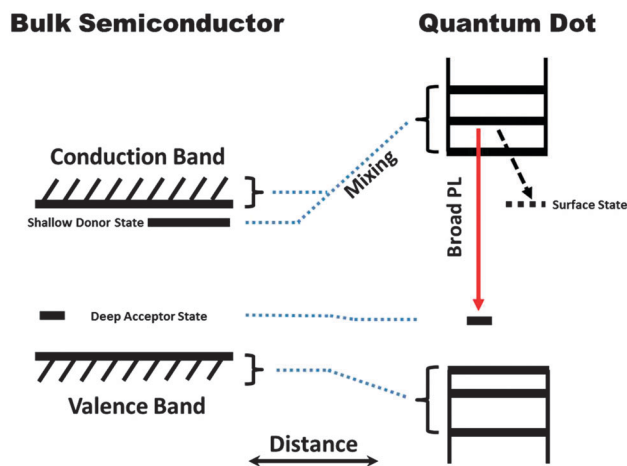

Fig. 7 Simplified schematic correlation diagram comparing electronic states of the bulk CIS with those of CIS QDs with assumed shallow donors and deep acceptors. Shallow donors are represented by a long line, indicating that the carriers trapped at shallow donors are more spatially delocalized than those trapped at deep acceptors. The energetic shifts of the conduction and valence band states in the QDs are not of equal magnitude in general, as shown in the figure.

the free electrons, which are delocalized over the whole QD, and holes, which are strongly localized at acceptors. It can be concluded that the dominant luminescence mechanism is free-to-bound recombination in CIS QDs, especially for the core/shell QDs, and the radiative and nonradiative processes in CIS QDs are related to the intrinsic and surface defects, respectively.

4 Conclusions

In this work, we have systematically investigated the optical properties of the synthesized CIS core and CIS/ZnS core/shell QDs. Both femtosecond TA and nanosecond time-resolved PL measurements give a strong indication that the emission in the CIS QDs is due to the radiative recombination between the free electrons and localized holes. We revealed that the TA dynamics in CIS QDs depended on the excitation densities, indicating that the trap-assisted Auger recombination is dominant in photocarrier dynamics under strong excitation. Besides this, we observed that the size-dependent PL decays took place over dozens of nanoseconds in CIS QDs. The PL dynamics exhibits size dependence because of the surface trapping in CIS QDs in which electrons quickly or slowly relax from the 1S states to the surface trap states. The surface trapping increases markedly and the trapping rates depend on the inverse of the QD radius: $1/\tau_{\text{trap}} \propto R^{-3.3}$. However, the free-to-bound radiative-recombination hardly depends on the QD size. Furthermore, the PL peaks shift toward longer wavelength as time proceeds because of the fast surface-trapping and the coexistent large inhomogeneous broadening in CIS QDs. The peak shift is less pronounced in well-passivated CIS/ZnS core/shell core QDs. Our findings provide information about the dynamical behavior of photocarriers, which is necessary to develop high-efficiency optoelectronic devices based on CIS QDs.

Acknowledgements

Notes and references

1 J. E. Jaffe and A. Zunger, *Phys. Rev. B: Condens. Matter Mater. Phys.*, 1983, **28**, 5822.

2 L. Li, A. Pandey, D. J. Werder, B. P. Khanal, J. M. Pietryga and V. I. Klimov, *J. Am. Chem. Soc.*, 2011, **133**, 1176.

3 H. Zhong, S. S. Lo, T. Mirkovic, Y. Li, Y. Ding, Y. Li and G. D. Scholes, *ACS Nano*, 2010, **4**, 5253.

4 B. Chen, H. Zhong, W. Zhang, Z. Tan, Y. Li, C. Yu, T. Zhai, Y. Bando, S. Yang and B. Zou, *Adv. Funct. Mater.*, 2012, **22**, 2081.

5 T.-L. Li, Y.-L. Lee and H. Teng, *Energy Environ. Sci.*, 2012, **5**, 5315.

6 H. McDaniel, N. Fuke, N. Makarov, J. Pietryga and V. Klimov, *Nat. Commun.*, 2013, **4**, 2887.

7 Z. Pan, I. Mora-Seró, Q. Shen, H. Zhang, Y. Li, K. Zhao, J. Wang, X. Zhong and J. Bisquert, *J. Am. Chem. Soc.*, 2014, **136**, 9203–9210.

8 W.-S. Song and H. Yang, *Appl. Phys. Lett.*, 2012, **100**, 183104.

9 W. Zhang, Q. Lou, W. Ji, J. Zhao and X. Zhong, *Chem. Mater.*, 2014, **26**, 12041212.

10 J.-H. Kim and H. Yang, *Opt. Lett.*, 2014, **39**, 5002.

11 M. Panthani, T. Khan, D. Reid, D. Hellebusch, M. Rasch, J. Maynard and B. Korgel, *Nano Lett.*, 2013, **13**, 4294.

12 T. Pons, E. Pic, N. Lequeux, E. Cassette, L. Bezdetnaya, F. Guillemin, F. Marchal and B. Dubertret, *ACS Nano*, 2010, **4**, 2531.

13 L. Li, T. Daou, I. Texier, T. Chi, N. Liem and P. Reiss, *Chem. Mater.*, 2009, **21**, 2422.

14 K. T. Yong, I. Roy, R. Hu, H. Ding, H. Cai, J. Zhu, X. Zhang, E. J. Bergey and P. N. Prasad, *Integr. Biol.*, 2010, **2**, 121.

15 S. Castro, S. Bailey, R. Raffaelle, K. Banger and A. Hepp, *J. Phys. Chem. B*, 2004, **108**, 12429.

16 H. Zhong, Y. Zhou, M. Ye, Y. He, J. Ye, C. He, C. Yang and Y. Li, *Chem. Mater.*, 2008, **20**, 6434.

17 J. Zhang, R. Xie and W. Yang, *Chem. Mater.*, 2011, **23**, 3357.

18 Y.-K. Kim, S.-H. Ahn, K. Chung, Y.-S. Cho and C.-J. Choi, *J. Mater. Chem.*, 2012, **22**, 1516.

19 J. Park and S.-W. Kim, *J. Mater. Chem.*, 2011, **21**, 3745.

20 X. Tang, W. Cheng, E. Choo and J. Xue, *Chem. Commun.*, 2011, **47**, 5217.

21 L. Trizio, M. Prato, A. Genovese, A. Casu, M. Povia, R. Simonutti, M. Alcocer, C. D'Andrea, F. Tassone and L. Manna, *Chem. Mater.*, 2012, **24**, 2400.

22 W. Zhang and X. Zhong, *Inorg. Chem.*, 2011, **50**, 4065.

23 T.-L. Li, Y.-L. Lee and H. Teng, *J. Mater. Chem.*, 2011, **21**, 5089.

24 H. McDaniel, N. Fuke, J. Pietryga and V. Klimov, *J. Phys. Chem. Lett.*, 2013, **4**, 355.

25 Y. Hamanaka, T. Ogawa, M. Tsuzuki and T. Kuzuya, *J. Phys. Chem. C*, 2011, **115**, 1786.

26 B. Mao, C.-H. Chuang, J. Wang and C. Burda, *J. Phys. Chem. C*, 2011, **115**, 8945.

27 T. Omata, K. Nose, K. Kurimotoa and M. Kita, *J. Mater. Chem. C*, 2014, **2**, 6867.

28 J. Sun, D. Zhu, J. Zhao, M. Ikezawa, X. Wang and Y. Masumoto, *Appl. Phys. Lett.*, 2014, **104**, 023118.

29 V. I. Klimov, S. Hunsche and H. Kurz, *Phys. Rev. B: Condens. Matter Mater. Phys.*, 1994, **50**, 8110.

30 V. I. Klimov, A. A. Mikhailovsky, D. W. McBranch, C. A. Leatherdale and M. G. Bawendi, *Science*, 2000, **287**, 1011.

31 A. Cohn, A. Schimpf, C. Gunthardt and D. Gamelin, *Nano Lett.*, 2013, **13**, 1810.

32 C. J. Stolle, R. D. Schaller and B. A. Korgel, *J. Phys. Chem. Lett.*, 2014, **5**, 3169.

33 P. T. Landsberg, *Appl. Phys. Lett.*, 1987, **50**, 745.

34 P. T. Landsberg, *Recombination in Semiconductors*, Cambridge University Press, Cambridge, England, 1991.

35 Y. Yamada, H. Yasuda, T. Tayagaki and Y. Kanemitsu, *Phys. Rev. Lett.*, 2009, **102**, 247401.

11988 | *Phys. Chem. Chem. Phys.*, 2015, **17**, 11981–11989

This journal is © the Owner Societies 2015

36 Y. Jang, T. Badcock, D. Mowbray, M. Skolnick, J. Park, D. Lee, H. Liu, M. Hopkinson, R. Hogg and A. Andreev, *Appl. Phys. Lett.*, 2008, **93**, 101903.

37 W. P. Dumke, *Phys. Rev.*, 1963, **132**, 1998.

38 M. Jones, S. S. Lo and G. D. Scholes, *Proc. Natl. Acad. Sci. U. S. A.*, 2011, **106**, 3011.

39 S. L. Sewall, R. R. Cooney, K. E. H. Anderson, E. A. Dias, D. M. Sagar and P. Kambhampati, *J. Chem. Phys.*, 2008, **129**, 084701.

40 P. Rodney, A. Marchetti and P. Fauchet, *Phys. Rev. B: Condens. Matter Mater. Phys.*, 2000, **62**, 4215.

41 J. Sun, J. Zhao and Y. Masumoto, *Appl. Phys. Lett.*, 2013, **102**, 053119.

42 H. Y. Ueng and H. L. Hwang, *J. Appl. Phys.*, 1987, **62**, 434.

43 H. Y. Ueng and D. Y. Chang, *Jpn. J. Appl. Phys.*, 1993, **32**, 469.

44 L. Brus, *J. Phys. Chem.*, 1986, **90**, 2555.

45 L. Brus, *J. Phys. Chem.*, 1986, **90**, 3393.

46 A. Ishizumi and Y. Kanemitsu, *J. Phys. Soc. Jpn.*, 2010, **79**, 093706.